PACS: 62.20.Fe, 81.40.f

S.V. Dobatkin

NANO- AND SUBMICROCRYSTALLINE STEELS PROCESSED BY SEVERE PLASTIC DEFORMATION

A.A. Baikov Institute of Metallurgy and Materials Science, Russian Academy of Sciences
Moscow, Russia

The aim of this paper is to consider the features of structure evolution during severe plastic deformation (SPD) of steels and its influence on mechanical properties. The investigations have been carried out mainly on low-carbon steels as well as on austenitic stainless steels after SPD by torsion under high pressure (HPT) and equal-channel angular pressing (ECAP). Structure formation dependences on temperature deformation conditions, strain degree, chemical composition, initial state and pressure are considered. The role of phase transformations for additional grain refinement, namely, martensitic transformation, precipitation of carbide particles during SPD and heating is underlined.

1. Introduction

At present, a great attention is paid to the processes of SPD due to the opportunity of the formation of nano- (grain size less than 100 nm) and submicrocrystalline (grain size between 100 and 1000 nm) structures upon deformation [1,2]. The method consists in severe deformation, at relatively low temperatures (below $(0.3–0.4)T_m$), under high applied pressures and provides bulk pore-free nano- and submicrocrystalline metals and alloys [2]. Conventional deformation methods, such as rolling, drawing, pressing, etc., reduce the cross-sectional area of a billet and do not allow one to obtain a high strain and grain refinement. Nontraditional methods, such as torsion under high hydrostatic pressure, equal-channel angular pressing, multiaxial deformation, alternating bending, accumulative roll bonding, twist extrusion, and so on, allow one to deform a billet without changing the cross-sectional area and to reach desirable high strain and grain refinement. Structures obtained during SPD have specific features: small size of grains down to nanolevel, low density of free dislocations, high-angle misorientation of the grains, and high-energy and nonequilibrium state of grain boundaries [2]. These structures lead to changes in physical and mechanical properties: a significant increase in the strength at good ductility, an increase in the wear resistance, and high-speed and low-temperature superplasticity [2].

Most works are related to the SPD of pure metals and rather plastic alloys. The use of SPD for commercial steels has been poorly studied. Moreover, now it is difficult to widely apply severe plastic deformation in industry. Nevertheless, it is important to study the limiting structural states of commercial steels and a combination of their mechanical and service properties.

The purpose of this paper is to consider the features of structure formation during SPD and mechanical properties of austenitic stainless and low-carbon steels.

2. Factors affecting the structure formation during SPD

2.1. Temperature

It is well known that hot deformation can cause grain refinement due to the occurrence of dynamic recrystallization. The lower is the temperature, the finer are the grains, but, at the same time, the higher is the degree of deformation required for the beginning of dynamic recrystallization (Fig. 1). It would seem that the smallest grain size can be obtained at room temperature, but this requires the degree of deformation which cannot be realized with conventional deformation schemes, such as rolling, extrusion, forging, etc. In reality, the grained structure with high-angle grain boundaries was obtained at room temperature by using methods of severe plastic deformation, such as torsion under high hydrostatic pressure (HPT) and ECAP. However, the formation of high-angle boundaries, i.e., the process of recrystallization is thermally activated and requires elevated temperatures. Now it is already well established that room-temperature SPD under the high pressure initiates the diffusion-controlled dislocations climb processes [3]. Just these processes are responsible for the formation of new grains. Is this process a dynamic recrystallization? In our opinion – yes, it is, since, the new grains appear in the deformed matrix, they belong to the matrix phase, but are substantially more perfect and separated from other grains by high-angle boundaries [4].

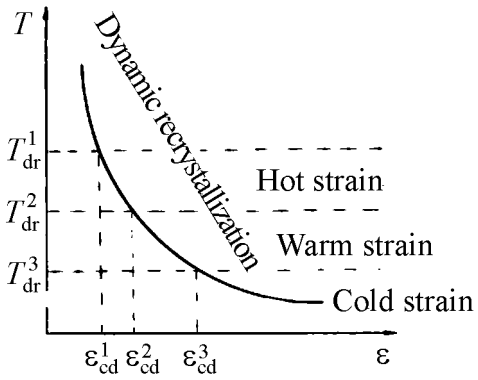

Fig. 1. Dependence of critical strain for dynamic recrystallization on temperature

Thus, lowering the SPD temperature to room temperature, we can refine the grain structure to the nanosize scale.

2.2. Degree of strain

It is conventionally assumed that the formation of predominantly nanocrystalline structure upon SPD at a lowered temperature corresponds to the steady-stage portion in the graph of the dependence of microhardness on the degree of strain, i.e., to a true degree of strain $\varepsilon \approx 5$–7 [2]. However, one should take into account that the degree of strain, which causes the formation of new grains with high-

angle boundaries, depends on the stacking fault energy and the degree of alloying of the material. The required degree of strain increases with decreasing stacking fault energy and increasing degree of alloying. For example, the formation of submicrocrystalline structure upon HPT in armco-iron begins earlier than in the ferritic steel 0.08% S–18% Cr–1.0% Ti with the same bcc lattice[5].

2.3. Strain rate

An increase in the strain rate leads to the grain refinement. However, it is unreasonable to increase the strain rate in the case of SPD at room temperature. First, upon cold deformation, unlike hot deformation, an increase in strain rate insignificantly decreases the grain size. Second, an increase in strain rate causes the formation of surface cracks and the premature failure of the sample, especially upon ECAP, because of the contact of the sample with the internal right angle of the die.

2.4. Chemical composition

Nanostructure formation depends on chemical composition. During severe deformation at room temperature, the alloying facilitates grain refinement by slowing down the diffusion (under high pressure, an appreciable diffusion takes place even at room temperature [3]), by reducing the stacking fault energy, as well as by the necessity to apply higher deforming stresses. For example, after SPD by torsion under high pressure at room temperature the grain size in armco-iron is ~ 200 nm just as in ferritic stainless 18% Cr–Ti steel – ~150 nm [5]. Changes of chemical composition could initiate phase transformations and change the structure.

2.5. Initial state

It is shown that the metastable nonequilibrium initial state (metastable austenite, quenched oversaturated solid solution, etc.) results in highest grain refinement during SPD at the expense of phase transformations (martensitic transformations, precipitation and dissolution of carbides, etc.) and often helps to achieve the nanoscale grain size level [6]. Austenitic stainless Cr–Ni steel undergoes martensitic transformation during SPD at room temperature [5–7]. Martensitic transformation leads to additional grain refinement and the dual phase austenitic–martensitic nanocrystalline structure exhibits higher thermal stability because the grain growth of one phase constituent is suppressed by the other constituent, and vice versa.

Severe deformation of an oversaturated solid solution can induce its decomposition in the course of deformation. Decomposition of the solid solution can also be initiated before and after severe deformation. The second-phase particles that have precipitated during heat treatment inhibit grain growth. Severe low-temperature deformation can lead to dissolution of the precipitates simultaneously with the formation of nanostructure. The possibility for dissolving cementite Fe_3C particles was demonstrated in cold rolling of carbon steels with high reductions [8]. Recently, the dissolution of carbides in quenched low-carbon 0.2% C–Mn–B steel [9], and complete dissolution of cementite Fe_3C in high-carbon 1.2% C steel [10] have been shown. Subsequent reheating can then result in reprecipitation of

the disperse particles and in stabilization of nanostructure. It should be noted that the dissolution of the second-phase particles and their ability to stabilize the structure depend on the size and volume fraction of precipitates.

2.6. Pressure

Structure and, correspondingly, strengthening depend on the pressure applied upon SPD. For example, for the low-carbon 0.1% C–Mn–Si steel, just as for the high-carbon 0.8% C–6% W–5% Mo steel, an increase in pressure from 4 to 10 GPa upon room-temperature HPT leads to a significant strengthening (Fig. 2). Moreover, for the initially quenched state, the strengthening and the structure refinement are higher than those observed for the initially annealed structure.

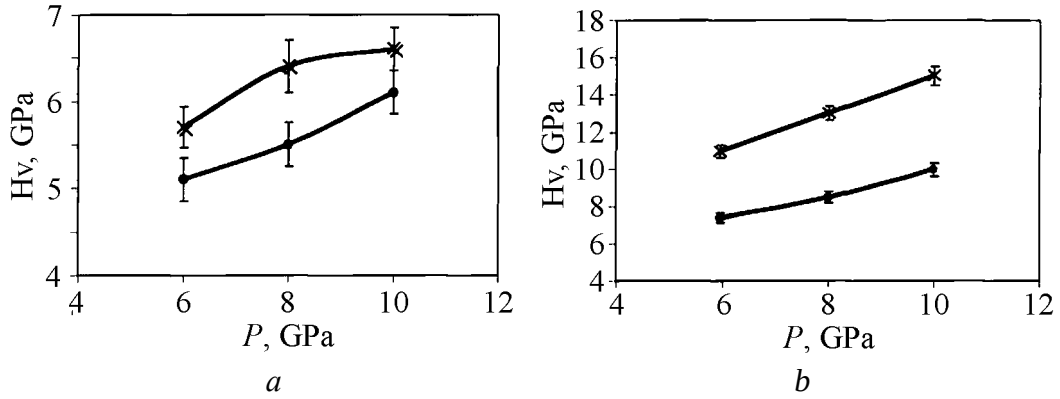

Fig. 2. Microhardness dependence on pressure during SPD by HPT at room temperature with $\varepsilon \approx 6$: *a* – low-carbon 0.1% C–Mn–Si steel (S. Dobatkin et al, 2001); *b* – high-carbon 0.8% C–6% W–5% Mo steel (S. Dobatkin, M. Zehetbauer et al, 2001). Initial state: × – as-quenched, ● – as-annealed

3. Structure and properties of steels after SPD

3.1. Austenitic stainless steels

Different structures can be obtained depending on experimental scheme. The limiting structural states are generally realized upon HPT since, in this case, the applied pressure (up to 10 GPa) allows one to reach a high strain degree [4]. The ECAP as one of the most advantageous SPD methods allows to prepare nano- and submicrocrystalline samples as large as 20–40 mm in diameter and 100–150 mm long [2,11,12]. The pieces of such size can be widely used for medical tools and implants; in particular, they are already tested for titanium [2].

Room-temperature deformation of 0.08% C–18.3% Cr–9.8% Ni–0.6% Ti austenitic steel by HPT (P = 6 GPa) on the samples of 10 mm diameter and 1 mm thick leads to the formation of separated structure elements with high-angle boundaries already at e = 4.3 (1 revolution) [5,7]. As a whole, the oriented structure, which is formed at the initial stages, is transformed into a rather equiaxed structure upon further deformation. The average size of structural elements is about 50 nm in the 0.08% C–18.3% Cr–9.8% Ni–0.6% Ti steel after deformation

by HPT to e = 5.8 (5 revolutions) (Fig. 3). The character of the selected area electron-diffraction (SAED) pattern generally indicates a high-angle misorientation at the boundaries. Therefore, we can define the obtained structure as nanocrystalline.

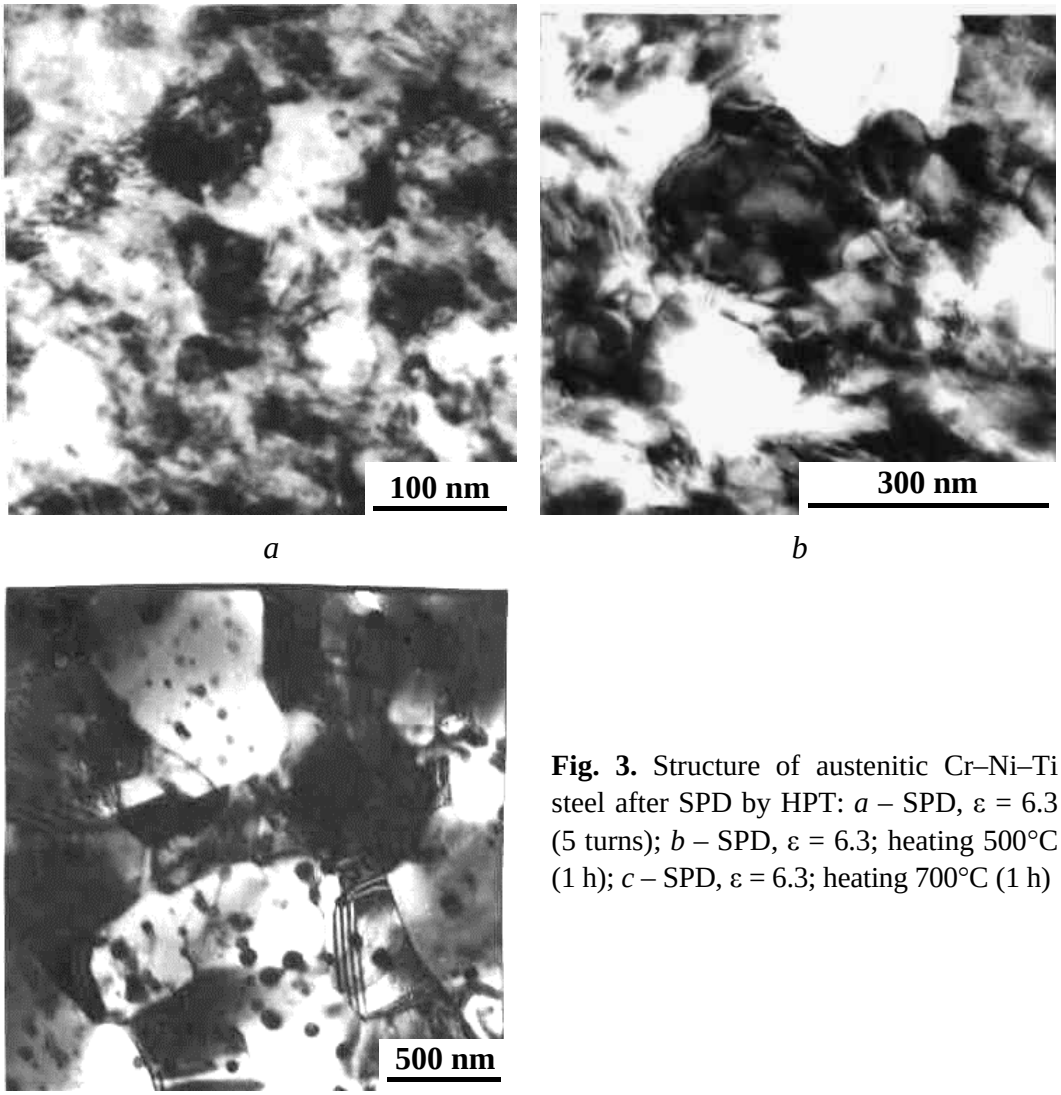

a *b* *c*

Fig. 3. Structure of austenitic Cr–Ni–Ti steel after SPD by HPT: *a* – SPD, ε = 6.3 (5 turns); *b* – SPD, ε = 6.3; heating 500°C (1 h); *c* – SPD, ε = 6.3; heating 700°C (1 h)

Severe plastic deformation induces the martensitic transformation in austenitic steels [5–7]. The martensite content in the 0.08% C–18.3% Cr–9.8% Ni–0.6% Ti steel sample was 50% already at e = 4.3 (1 revolution) and ~ 60% at e = 5.8 (5 revolutions) (Fig. 4) [5]. Not only $\gamma \rightarrow \alpha$, but also $\gamma \rightarrow \varepsilon \rightarrow \alpha$ transformation was revealed. The X-ray diffraction data on the volume fraction of martensite were obtained with no account for texture [5,6]. As we determined the martensite content with allowance for texture formed upon deformation by torsion [7], the same samples after e = 5.8 (5 revolutions) revealed 80% rather than 60% martensite shown

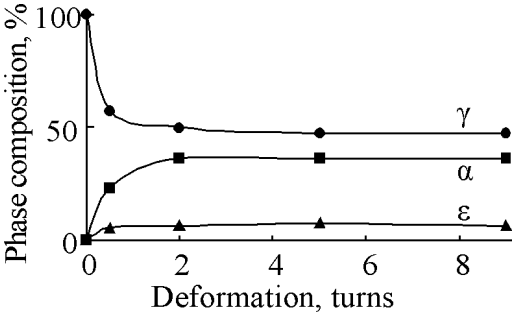

Fig. 4. Changes of phase composition during SPD by HPT of austenitic 0.08% C–18.3% Cr–9.8% Ni–0.6% Ti steel

earlier [5]. In general, we note that the difference in the martensite content in austenitic steels subjected to SPD is caused not only by the deformation scheme and applied pressure, but also, to a greater extent, by the technique of the α-phase content determination.

In any case, SPD leads to the formation of a two-phase austenitic-martensite structure, which should increase the thermal stability of the obtained nanocrystalline steel. Upon heating the nanocrystalline 0.08% C–18.3% Cr–9.8% Ni–0.6% Ti steel after SPD by HPT, the initial grain size of 50 nm remains virtually unchanged up to a temperature of 400°C. The grain size slightly increases (to 250 nm) at 500°C and begins intensely growing at temperatures above 600°C (Fig. 3) [7].

This corresponds to the changes in the volume fractions of phase constituents upon heating [7]. The martensite fraction begins decreasing upon heating above 400°C. After heating to 550°C, the phase composition corresponds to the percentage of 50:50%. This still suppresses the intense grain growth, which begins at 600°C, when the austenite content is ~ 80%. Upon heating the nanocrystalline steel to 600°C, the grain size is retained in a submicrocrystalline range, remaining below 1 μm. After heating to 800°C, the grain size was determined by metallographic examination to be ~ 7 μm.

To determine the mechanical characteristics after SPD, the bulk samples were subjected to room-temperature deformation by ECAP, since the samples deformed by HPT are not suitable for standard mechanical tests.

An opportunity to deform a sample in the ECAP die without failure is generally determined by the construction of this die, which is characterized by a decreased friction in the input channel and a backpressure in the output channel. The die used in [7] allowed to deform a sample of 0.07% C–17.3% Cr–9.2% Ni–0.7% Ti austenitic steel of 20 mm diameter and 80 mm long for four passes, i.e. $N = 4$ (one pass at an angle of 90° between channels and three passes at an angle of 120°), to a true deformation $e = 3.2$ at room temperature.

The limiting deformation achieved by ECAP of 0.07% C–17.3% Cr–9.2% Ni–0.7% Ti steel is much lower than that achievable by HPT. For this reason, we failed to obtain an equiaxed structure after ECAP. Oriented structure consisting of elements of 100–250 nm in size (a distance between subgrain or grain boundaries) and separated equiaxed grains of the same size were observed. Such oriented structure elements are presented by shear and deformation bands, twins, martensitic plates, and oriented subgrains (cells) [13]. It is difficult to resolve the structure type in such a fine structure. The oriented structures frequently cross each other at an angle. The nucleation of equiaxed grains can occur also through the cellular structure. With increasing strain degree, the fraction of the grained structure increases, but even at $N = 4$ ($e = 3.2$), the structure remains far from being perfect.

Unlike HPT, the ECAP under the mentioned conditions induces a weak martensitic transformation, which becomes more active only at $N = 4$, leading to the formation of 45% martensite [7].

Even the imperfect and oriented submicrocrystalline structure of 0.07% C–17.3% Cr–9.2% Ni–0.7% Ti steel after ECAP provides a good combination of mechanical properties. Already at $N = 2$, the yield strength (YS) is 990 MPa at an elongation of 13% (Table 1) [7]. The further deformation up to $N = 4$ monotonously increases the YS up to 1315 MPa at elongation (EL) = 11%. To obtain a perfect nano- or submicrocrystalline structure, one should either increase the degree of deformation, or heat the obtained structure. High degree of the achievable deformation and a high pressure used in [14] resulted in a more perfect grained structure with a grain size of ~ 100 nm and, correspondingly, a higher plasticity (EL = 27.5%) at a somewhat higher strength (YS = 1340 MPa).

Table 1

Mechanical properties of 0.07% C–17.3% Cr–9.2% Ni–0.7% Ti austenitic steel after ECAP at room temperature and $N = 2–4$

State	UTS	YS	EL	RA
	MPa		%	
Initial	570	250	58	77
2 passes	1080	990	13	64
3 passes	1180	1120	13.5	56.5
4 passes	1400	1315	11	58

3.2. Low-carbon steels

3.2.1. Cold ECAP

A submicrocrystalline structure in bulk billets of low-carbon steels can be produced by ECAP at reduced deformation temperatures. However, the lower the deformation temperature, the higher the deformation required for the formation of high-angle boundaries, i.e., new grains [15]. The maximum achievable deformation without failure of a sample upon ECAP depends substantially on the equipment used, a decrease in the friction in the channels, and the backpressure [11,12]. Upon cold ECAP, low-carbon steels can only be subjected to two or three deformation cycles at the most efficient angle of channel intersection (90°) without the failure of a sample, which is insufficient to produce a developed grain structure [16,17]. The structure produced consists of cellular and subgrain regions with a high dislocation density and a small number of individual submicron grains.

Low-carbon 0.1% C–1.6% Mn–0.1% V–0.08% Ti steel in two initial states: the ferritic-pearlitic state after hot rolling and the martensitic (bainitic) state produced by quenching from 925ºC (30 min) was studied [18]. ECAP was performed at a channel intersection angle of 90° on samples 5 mm in diameter and 30 mm long in two cycles ($N = 2$) at room temperature for the initially ferritic-pearlitic state and at $N = 2$ and $T_{def} = 400$ºC for the initially martensitic state, which corresponded to the maximum possible cold deformation without failure.

The cold ECAP of the hot-rolled and quenched samples of the 0.1% C–1.6% Mn–0.1% V–0.08% Ti steel at $N = 2$ results in a cellular and subgrain structure (Fig. 5,*a*,*d*). There are also areas with both an oriented structure and equiaxed structural elements, which contain separate grains with high-angle boundaries. After ECAP of this steel with the initially ferritic-pearlitic structure the spheroidization

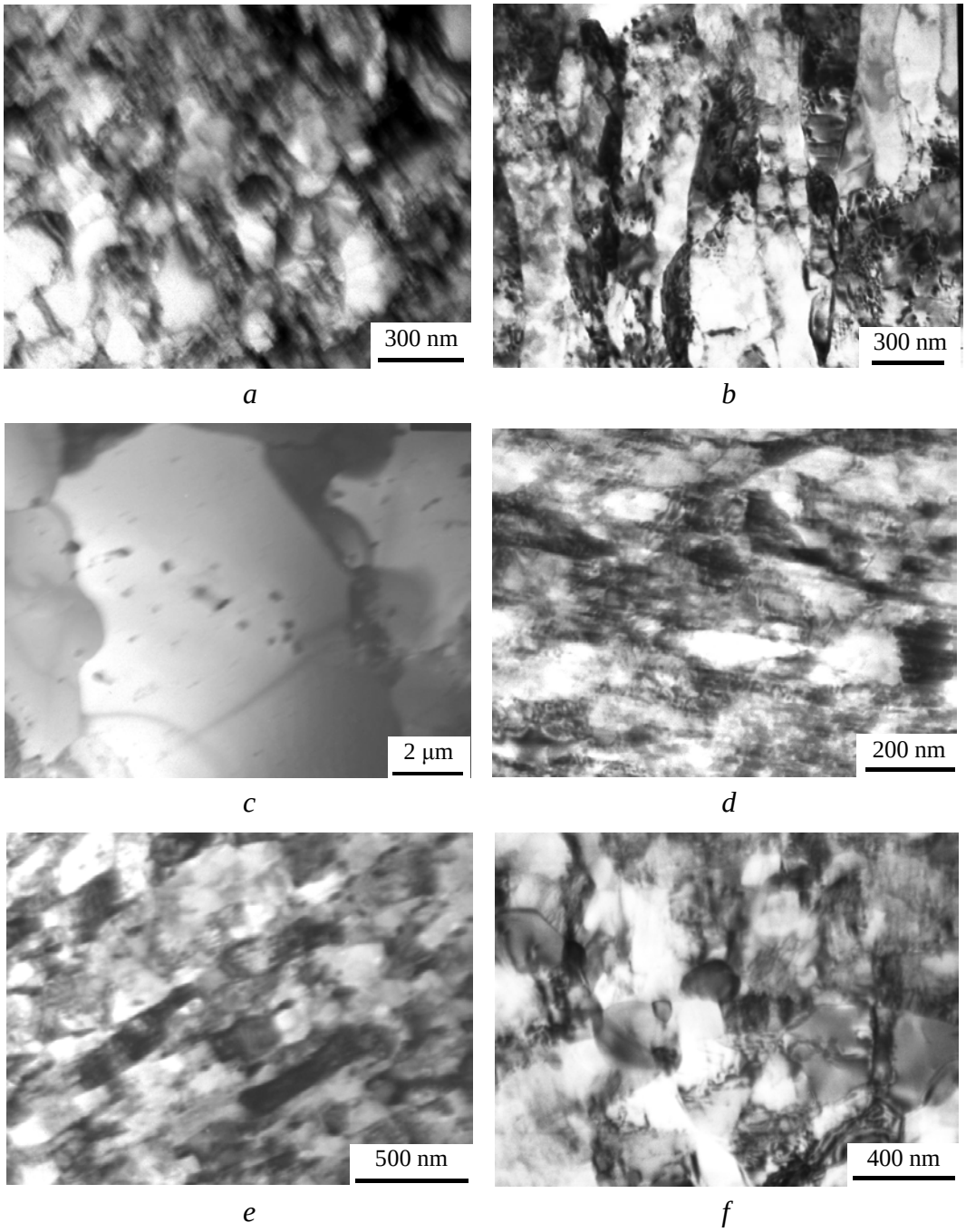

a *b* *c* *d* *e* *f*

Fig. 5. Structure of 0.1% C–1.6% Mn–0.1% V–0.08% Ti steel after cold ECAP and heating: *a*, *d* – ECAP; *b*–*e* – ECAP + 600ºC (10 min); *c*–*f* – ECAP + 700°C (10 min); *a*–*c* – initial ferritic-pearlitic state (before ECAP); *d*–*f* – initial martensitic (bainitic) state (before ECAP)

of the cementite plates was observed. The size of the structural elements is 150–350 nm. The fact that the structural elements in the quenched deformed samples are significantly smaller than in the hot-rolled deformed samples can be due to an initially higher dislocation density there. After 10-min heating of the deformed quenched sample at 600ºC, its structure becomes mixed: the partly polygonized (subgrain) structure has low-angle boundaries, whereas the partly submicrocrystalline structure has high-angle grain boundaries (Fig. 5,*e*). The fact that the boundaries are high-angle is indicated by the characteristic fringe contrast at the grain boundaries, which is observed upon an electron-microscopic examination, and by the appearance of individual reflections in diffraction rings. The structures are mainly oriented. Equiaxed grains and subgrains are, as a rule, formed inside oriented subgrains. As the temperature of heating of the 0.1% C–1.6% Mn–0.1% V–0.08% Ti steel with the initially quenched structure after ECAP increases from 600 to 700ºC, the structure becomes not so oriented and the fraction of grains and their sizes increase (Fig. 5,*f*). The size of the structural elements increases, on the average, from ~ 0.2 to ~ 0.3 μm. The regions with the oriented structure are retained in a totally equiaxed structure after heating at 700ºC. Heating after ECAP of the 0.1% C–1.6% Mn–0.1% V–0.08% Ti steel with the initially ferritic-pearlitic structure at 600ºC leads to the formation of an inhomogeneous structure (Fig. 5,*b*). This structure is mainly oriented and polygonized and has individual equiaxed grains and subgrains. Areas with a cellular structure having a high dislocation density are also retained. Heating of the hot-rolled samples after ECAP at 700°C results in a grain structure with a grain size of 6–12 μm (Fig. 5,*c*). Unlike heating of the deformed samples with ferritic-pearlitic structure of the 0.1% C–1.6% Mn–0.1% V–0.08% Ti steel at 700°C, the formation and retention of the submicrocrystalline structure with a grain size of ~ 300 nm upon heating of the quenched samples of this steel at 700°C after ECAP can be explained by, first, the higher homogeneity of the initial martensite (bainite) structure, second, the higher initial dislocation density, and third, the precipitation of fine uniformly distributed carbides upon heating.

After two ECAP cycles, the strength properties of the 0.1% C–1.6% Mn–0.1% V–0.08% Ti steel increase. Specifically, the yield strength is almost doubled: it increases from 510 to 1000 MPa for the initially hot-rolled samples and from 600 to 1110 MPa for the initially quenched samples (Table 2) [18]. Under these conditions, the ductility EL_{tot} changes only slightly for the initially hot-rolled samples and decreases for the initially quenched samples, which is likely due to a significant increase in the dislocation density. In the case of the initially hot-rolled samples, a decrease in the EL_{tot} induced by an increase in the dislocation density is likely to be compensated for by an increase in EL because of the fragmentation and spheroidization of carbides in the pearlite. Upon heating the 0.1% C–1.6% Mn–0.1% V–0.08% Ti steel after ECAP, the strength properties decrease but in different ways: for the hot-rolled samples, YS decreases by 22 and 42% upon heating at 600 and 700ºC, respectively, and by 10 and 27% for the quenched sam-

ples upon heating at the same temperatures, respectively. The YS of the quenched sample of the 0.1% C–1.6% Mn–0.1% V–0.08% Ti steel after ECAP, even upon heating at 600ºC, retains its high value (YS = 1015 MPa) at the ductility characteristics EL_{tot} = 28% and RA = 40%. The total elongation upon heating the 0.1% C–1.6% Mn–0.1% V–0.08% Ti steel after ECAP increases to EL_{tot} < 30%, except for heating of the hot-rolled sample at 700°C, when a completely grain structure with a grain size of 6–12 μm provides EL_{tot} = 39%. It should be noted that the values of uniform elongation EL_{uni} are high for the initially quenched samples after ECAP followed by heating and that those for the initially hot-rolled samples are low. The strength properties: ultimate tensile strength (UTS) and YS are substantially higher in the initially hot-rolled samples of the 0.1% C–1.6% Mn–0.1% V–0.08% Ti steel after room-temperature ECAP. From the standpoint of the grain–subgrain structure, we would expect the best combination of strength and ductility for the 0.1% C–1.6% Mn–0.1% V–0.08% Ti steel in the initially hot-rolled samples after ECAP followed by heating at 600ºC and in the initially quenched samples after ECAP and heating at 700ºC. In real practice, this combination is reached immediately after ECAP in the former case and after ECAP followed by heating at 600ºC in the latter case. Probably, apart from the grain–subgrain perfection and the dislocation density, the state of the carbides in the steel also substantially affects the set of mechanical properties.

Table 2

Mechanical properties of 0.1% C–1.6% Mn–0.1% V–0.08% Ti steel after cold ECAP and heating

Treatment	YS	UTS	EL_{uni}	EL_{tot}	RA
	MPa		%		
Hot rolling (HR)	510	525	2.1	24	39
HR + ECAP (20°C, *N* = 2)	1000	1030	3.4	23	50.6
ECAP + 10 min at 600°C	780	790	4.2	22.7	40.6
ECAP + 10 min at 700°C	585	670	–	39.1	–
Quenching (Q)	600	845	–	27	65.5
Q + ECAP (400°C, *N* = 2)	1110	1170	12	15.2	–
ECAP + 10 min at 600°C	1000	1015	11	28.2	39.7
ECAP + 10 min at 700°C	810	870	16.2	23.5	-

3.2.2. Warm ECAP

Three low-carbon 0.17%C, 0.21% C–0.89% Mn–0.78% Si–0.16% V and 0.23% C–1.24% Mn–0.75% Si steels were studied after warm ECAP [19]. The 0.17%C steel was subjected to ECAP in the hot-rolled state, whereas the 0.21% C–0.89% Mn–0.78% Si–0.16% V and 0.23% C–1.24% Mn–0.75% Si steels were previously annealed at 950°C for 30 min and subsequently cooled in a furnace. In all the cases, the steels had a ferritic-pearlitic structure. Warm ECAP of 0.17%C steel was performed at 500ºC, whereas the 0.21% C–0.89% Mn–0.78% Si–0.16%

V and 0.23% C–1.24% Mn–0.75% Si steels were pressed at 550ºC. The angle of intersection of the two channels was equal to φ = 90º. Samples 20 mm in diameter and 120 mm long were subjected to four passes $N = 4$; the angle of rotation of the samples about the longitudinal axis between each pass was equal to 180º (route *C*). These conditions provide alternating strain. Four passes under these conditions correspond to the maximum strain before failure.

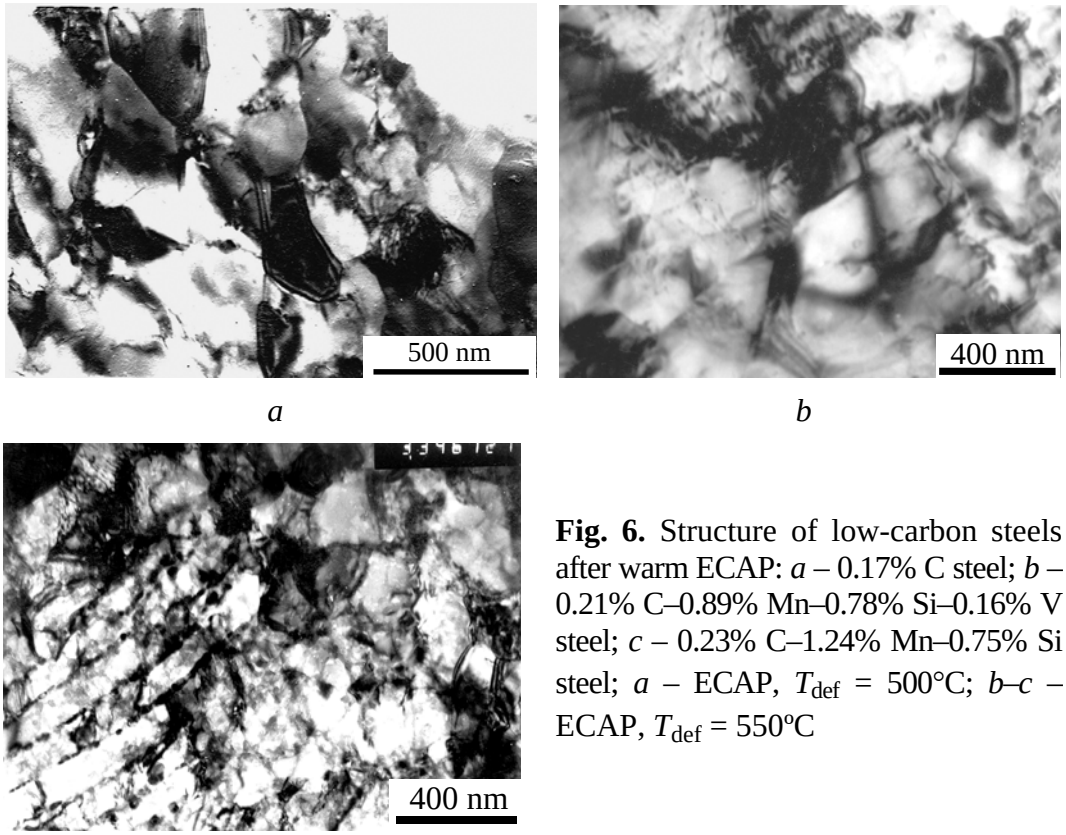

a *b* *c*

Fig. 6. Structure of low-carbon steels after warm ECAP: *a* – 0.17% C steel; *b* – 0.21% C–0.89% Mn–0.78% Si–0.16% V steel; *c* – 0.23% C–1.24% Mn–0.75% Si steel; *a* – ECAP, T_{def} = 500°C; *b*–*c* – ECAP, T_{def} = 550ºC

Using optical microscopy it is impossible to reveal a substructure in the strained elongated ferritic grains formed in the 0.17%C steel samples during warm ECAP at four passes. Electron microscopic study allowed to find both ferrite subgrains, which are formed within ferrite grains and are separated by low-angle boundaries, and a submicrocrystalline structure characterized by high-angle grain boundaries (Fig. 6,*a*). The substructure formed upon dynamic recovery is represented by two different structures, namely, oriented and relatively equiaxed structures. The submicrocrystalline structure is formed within both ferrite grains and pearlite colonies. In both cases, the sequence of formation of submicron grains is the same. Within both the oriented ferrite subgrains and the ferrite grains that are present between the cementite plates of pearlite colonies, transverse subboundaries are formed at the expense of lattice dislocations. Upon subsequent deformation, square or parallelogram subgrains become rounded; the subgrain boundary angle increases. Finally, the process of increasing the sub-

grain boundary angle is completed by the formation of submicron grains (less than 1 μm in size). Within the pearlitic colonies, this process is accompanied by the fragmentation and spheroidization of cementite plates. The sizes of the grains formed in ferrite and pearlite are different and determined by the distance between oriented subboundaries in the ferrite (0.3–0.4 μm) and the distance between cementite plates (0.1–0.2 μm) in the pearlite colonies, respectively. The average size of structural elements in the ferrite of the 0.17% C steel subjected to ECAP at T = 500ºC and N = 4 was measured in the cross-section for both the submicrocrystalline structure and the substructure; it was found to be 0.35 μm. The electron back-scattering data (EBSD) study confirmed the presence of two different structures with low- and high-angle grain boundaries that are formed within the initial elongated ferrite grains. It can be assumed that, under these conditions of ECAP, a completely submicrocrystalline structure can be formed after a larger number of passes. Using EBSD and TEM (Fig. 6,*b*,*c*), a similar data for the samples of the low-alloy low-carbon 0.21% C–0.89% Mn–0.78% Si–0.16% V and 0.23% C–1.24% Mn–0.75% Si steels subjected to warm ECAP at 550ºC and N = 4 were obtained: subgrain and grain structures characterized by structural elements 0.3–0.5 μm in size are formed. The steels differ in the fractions of low- and high-angle grain misorientations. All the samples have a mixed recovered + submicrocrystalline structure.

The partially submicrocrystalline structure leads to substantial hardening of the steels as evidenced by the similar values of YS and UTS (Table 3) as well as the yield drop in the stress–strain curve for the 0.17% C steel [20]. The yield strength of the 0.17% C steel (YS = 840 MPa) subjected to ECAP is higher than that of the hot-rolled steel by a factor of almost three; the samples exhibiting such high yield strength are characterized by rather large elongation (EL. = 10%) [19,20]. The low-alloy low-carbon 0.21% C–0.89% Mn–0.78% Si–0.16% V and 0.23% C–1.24% Mn–0.75% Si steels exhibit different hardening upon warm ECAP (Table 3) [19]. Even at N = 2, the 0.23% C–1.24% Mn–0.75% Si steel exhibits a high yield strength, which is virtually unchanged at N = 4. The 0.21% C–0.89% Mn–0.78% Si–0.16% V steel exhibits a substantial increase in yield strength at N = 4.

Table 3

Mechanical properties of low-carbon steels after warm and hot ECAP

Steel	T of ECAP, °C	φ (angle of channel intersection), deg	N	UTS	YS	EL	RA	KCV, MJ/m^2	
				MPa		%		+20	–40
0.17% C	500	90	4	–	–	–	–	0.39	–
0.21% C–0.89% Mn–0.78% Si–0.16% V	550	90	4	1120	1110	8	40	0.55	0.15
	750	110	8	850	820	15	–	2.52	–
		90	4	975	905	13	–	2.0	1.2
0.23% C–1.24% Mn–0.75% Si	550	90	4	1005	1000	11	44	0.21	0,14
	750	110	8	875	870	12	–	2.19	1.65

The yield strength of the 0.21% C–0.89% Mn–0.78% Si–0.16% V steel subjected to warm ECAP is higher than that of the 0.23% C–1.24% Mn–0.75% Si steel and is equal to 1100 MPa. In this case, its ductility is equal to 8–10% (Table 3). Unfortunately, the steels with the partially submicrocrystalline structure are characterized by a low impact toughness KCV at both +20 and –40°C (Table 3). It is likely that the low impact toughness of the steels can be due to both the mixed structure with a high density of dislocations in subgrains and the low size of structural elements, which specifies similar values of YS and UTS.

3.2.3. Hot ECAP

The 0.21% C–0.89% Mn–0.78% Si–0.16% V- and 0.23% C–1.24% Mn–0.75% Si steels were subjected to hot ECAP: T = 750ºC, N =4, φ = 90º and T = 750ºC, N = 8, φ = 110º. The degree of deformation reached after four and eight passes, which was calculated using the shear-strain intensity and the Mises equivalent strain, was equal to ~ 4.6 and ~ 6.5, respectively [19]. The calculations show that, if the angle between the two channels satisfies the inequality 90° < φ < 120º, the average pressure and total force upon simple shear are lower than the corresponding parameters of the process of equivalent direct pressing by factors of two to three and 5–15, respectively [11]. The samples were heated to the deformation temperature and held for 30 min. The equipment used for ECAP was heated to 500–550ºC. After each pass at 750ºC, the sample, whose surface was slightly cooled, was held in a furnace at 750ºC for 10–15 min to level off the temperature. Because of this, the total true strain was lower than the calculated value owing to static polygonization and possible recrystallization upon holding in the furnace between passes.

Thus, hot ECAP was performed at 750°C using two tools with the angles of intersection of two channels φ = 110º (N = 8) and φ = 90º (N = 4). In the former case, it was produced a mixed structure consisting of recrystallized 0.3–6 μm grains and ~ 0.5 μm subgrains, which was confirmed by both TEM and EBSD analysis. The structure formed in the 0.21% C–0.89% Mn–0.78% Si–0.16% V and 0.23% C–1.24% Mn–0.75% Si steels after hot ECAP at φ = 110° provides their hardening to YS > 800 MPa at an EL = 10–15%. Moreover, the samples exhibit a rather high impact toughness at +20 and –40ºC (Table 3). Upon hot ECAP at φ = 90° (N = 4), a polygonized structure is predominantly formed, thus providing higher hardening; the steel exhibits YS = 905 MPa and EL = 13% at a high impact toughness (Table 3). It is known that the degree of deformation needed for dynamic recrystallization decreases with increasing deformation temperature. Therefore, a completely recrystallized grain structure can be expected to form at a very high degree of deformation; it is calculated to be ε = 4.6 at = 90° and ε = 6.5 at = 110°. It is likely that the calculated degree of deformation does not correspond to the real degree of deformation because of static polygonization and, possibly, recrystallization that occur upon heating between ECAP passes. Thus, we failed to produce a uniform submicrocrystalline structure with a grain size of less than 1 μm by hot ECAP. However, the formation of a predominantly subgrain structure allowed us to substantially increase the impact toughness (at +20 and –40ºC) of the steels (as

the impact toughness (at +20 and –40ºC) of the steels (as compared to the steels after warm ECAP) at high retained hardening (Table 3).

Conclusion

Severe plastic deformation of steels results in grain refinement down to nanoscale. Structure is characterized by low density of internal dislocation and non-equilibrium state of grain boundaries. Such structure leads to high strength and sufficient ductility. Bulk nano- and submicrocrystalline steels in equilibrium state could be obtained by SPD and subsequent heating. A wide application of bulk nanomaterials is thought to be limited by the following causes: the whole set of mechanical and service properties, including fracture toughness, impact toughness, fatigue strength, corrosion resistance, etc., are poorly known; the sizes of prepared billets are relatively small; the production cost is high; there are no industrial technologies for producing bulk products with a homogeneous structure.

1. *Investigations* and Applications of Severe Plastic Deformation, T.C. Lowe, R.Z. Valiev (eds.), Kluwer Academic Publishing, Dordrecht, The Netherlands (2000).
2. *R.Z. Valiev, I.V. Alexandrov*, Nanostructured Materials Obtained by Severe Plastic Deformation, Logos, Moscow (2000) (in Russian).
3. *V.M. Farber*, MiTOM N 8, 3 (2002) (in Russian).
4. *S.S. Gorelik, S.V. Dobatkin, L.M. Kaputkina*, Recrystallization of Metals and Alloys, MISIS, Moscow (2005) (in Russian).
5. *S.V. Dobatkin, R.Z. Valiev, L.M. Kaputkina et al.*, Proc. Fourth International Conference On Recrystallization and Related Phenomena (REX'99), Tsukuba City, Japan, 1999, T. Sakai, H.G. Suzuki (eds.), JIM **13**, 907 (1999).
6. *S.V. Dobatkin*, Ultrafine Grained Materials II, Y.T. Zhu, T.G. Langdon, R.S. Mishra, S.L. Semiatin, M.J. Saran, T.C. Lowe (eds.), TMS (2002), p. 183–192.
7. *O.V. Rybal'chenko, S.V. Dobatkin, L.M. Kaputkina et al.*, Mat. Sci. Eng. **A387–389**, 244 (2004).
8. *V.N. Gridnev, V.G. Gavrilyuk*, Metallofizika, **4**, N 3, 74 (1982) (in Russian).
9. *M.V. Degtyarev, T.I. Chashchukhina, L.M. Voronova et al.*, Fiz. Met. Metalloved. **77**, N 2, 141 (1994) (in Russian).
10. *A.V. Korznikov, Yu.V. Ivanisenko, I.M. Safarov et al.*, Metally N 1, 91 (1994) (in Russian).
11. *V.M. Segal, V.I. Reznikov, V.I. Kopylov et al.*, Structure Formation in Metals, Nauka i Tekhnika, Minsk (1994) (in Russian).
12. *V. Segal*, Mater. Sci. Eng. **338A**, 331 (2002).
13. *A.M. Patselov, V.P. Pilyugin, E.G. Chernyshov et al.*, Structure and Properties of Nanocrystalline Materials, N. Noskova, G. Taluts (eds.), Ekaterinburg (1999), p. 37–44 (in Russian).
14. *I.I. Kositsyna, V.V. Sagaradze, V.I. Kopylov*, FMM **88**, N 5, 84 (1999) (in Russian).
15. *S.V. Dobatkin*, Investigations and Applications of Severe Plastic Deformation, T.C. Lowe, R.Z. Valiev (Eds.), NATO Science Series, Kluwer Academic Publishers, The Netherlands (2000), p. 13–22.

16. *Y. Fukuda, K. Oh-ishi, Z. Horita, T. Langdon*, Acta Mater. **50**, 1359 (2002).
17. *J. Kim, I. Kim, D.H. Shin*, Scr. Mater. **45**, 421 (2001).
18. *S.M.L. Sastry, S.V. Dobatkin, S.V. Sidorova*, Metally N 2, 28 (2004) (in Russian).
19. *S.V. Dobatkin, P.D. Odesskii, R. Pippan et al.*, Metally N 1, 110 (2004) (in Russian).
20. *S.V. Dobatkin, R.Z. Valiev, N.A. Krasilnikov, V.N. Konenkova*, Proc. Fourth International Conference On Recrystallization and Related Phenomena (REX'99), Tsukuba City, Japan, 1999, T. Sakai, H.G. Suzuki (eds.), JIM **13**, 913 (1999).